LANGMUIR Article
Cite This: Langmuir 2019, 35, 3880−3886
pubs.acs.org/Langmuir

Equilibrium Drop Shapes on a Tilted Substrate with a Chemical Step

Ivan Dević, José M. Encarnación Escobar, and Detlef Lohse*

Physics of Fluids Group, Department of Applied Physics and J. M. Burgers Centre for Fluid Dynamics, University of Twente, P.O. Box 217, 7500 AE Enschede, The Netherlands

ABSTRACT: We calculate the equilibrium shape of a droplet sitting on a tilted substrate with a "chemical step", that is, different lyophilicity at the two sides of the step. This problem can be generalized to that of a droplet experiencing a body force, pushing it from the lyophilic part to the lyophobic part of the substrate. We present phase diagrams, in which we show for which droplet sizes there are dynamically inaccessible equilibrium shapes. We also identify what determines the threshold volume. While this given system was studied previously in the literature using contact angle hysteresis laws, we present the full static thermodynamical solution of the interfacial energy including the contact energy, while omitting the hysteresis effects from the contact line.

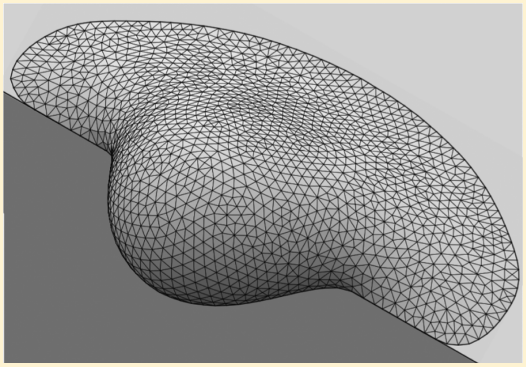

INTRODUCTION

Droplet wetting on chemically patterned surfaces has a wide range of applications and correspondingly raises both scientific[1−4] and industrial interest.[5−7] In the case of small-scale systems such as in catalysis[7] and in microfluidics,[5] the microscopic wetting properties dictate the macroscopic flow features of the system.[8] Although most of these processes are dynamical, there are also still a lot of unanswered questions when it comes to stable (equilibrium) droplet shapes.

Such an example is presented in Figure 1, where we show experimental side and bottom views of a stable water droplet on a "chemical step" in which the substrate was tilted by 30°, 40°, and 70°. With a "chemical step", we refer to a substrate with different hydrophobicity on the two sides of the step. It is visible that a small change in the substrate's slope results in a significant increase in the spreading from the hydrophilic toward the hydrophobic part of the substrate. Here, the droplet's length scale is larger than the capillary length scale so that gravity plays a role. In the literature, this problem is referred to as "sliding" droplet, though in the present case, the droplet was initially deposited on the chemical step; therefore, the occurrence of the sliding motion would indicate that there is no available equilibrium droplet shape.

While in experiment details of the droplet spreading and its shape depend on small-scale and hard-to-control surface heterogeneities, leading to pinning effects and hysteresis,[1−3,9] the present problem can be generalized to a droplet sitting at a chemical step and at the same time experiencing a body force. This body force can have a component parallel to the surface and a component perpendicular to the surface. In the case of a large droplet on a plate tilted by the angle α, these two corresponding force (per unit mass) components are simply $g \sin \alpha$ and $g \cos \alpha$. The case of a droplet much smaller than the capillary length (so that gravity does not play a role) can also be treated within this scheme: then, the normal force component $g \cos \alpha$ can be thought of as being negligible, while the parallel component $g \sin \alpha$ can simply be thought of as a constant body force parallel to the plate. In this paper, we will perform numerical analysis for both cases, that is, with and without normal force.

To obtain the equilibrium shape of a sessile droplet, by definition, one has to minimize its interfacial energy. The sessile droplet shape on a flat homogeneous substrate is governed by two principles: (i) the droplet interface has a constant mean curvature which is a function of the droplet volume (Young−Laplace equation) and (ii) the contact angle is uniquely defined via three separate surface tensions on the three-phase contact line (Young's law). On a chemically patterned substrate, the droplet contact energy and the contact angles depend on the location of the contact area. While the equilibrium shapes of droplets on such surfaces are visually very distinct from the spherical cap case on homogeneous substrates, the very same two principles (i) and (ii) still govern these shapes.[10−14]

Note that in this paper, we focus on droplets whose length scale is comparable to the length scale of the chemical pattern. Then, from the perspective of the droplet, the substrate can be considered as strongly heterogeneous.[15−17] To obtain the droplet equilibrium shape in that regime, numerical tools must be employed such as the gradient descent methods,[10−12,18] Monte-Carlo calculations,[19] or molecular dynamics simulation.[20]

In this paper, we will use Surface Evolver,[21,22] the free gradient descent software, to calculate the stable droplet shape on a substrate with a chemical step and experiencing a body force, as shown in Figure 2 for the case of a droplet on a tilted

Received: October 22, 2018
Revised: February 12, 2019
Published: February 14, 2019

DOI: 10.1021/acs.langmuir.8b03557
Langmuir 2019, 35, 3880−3886

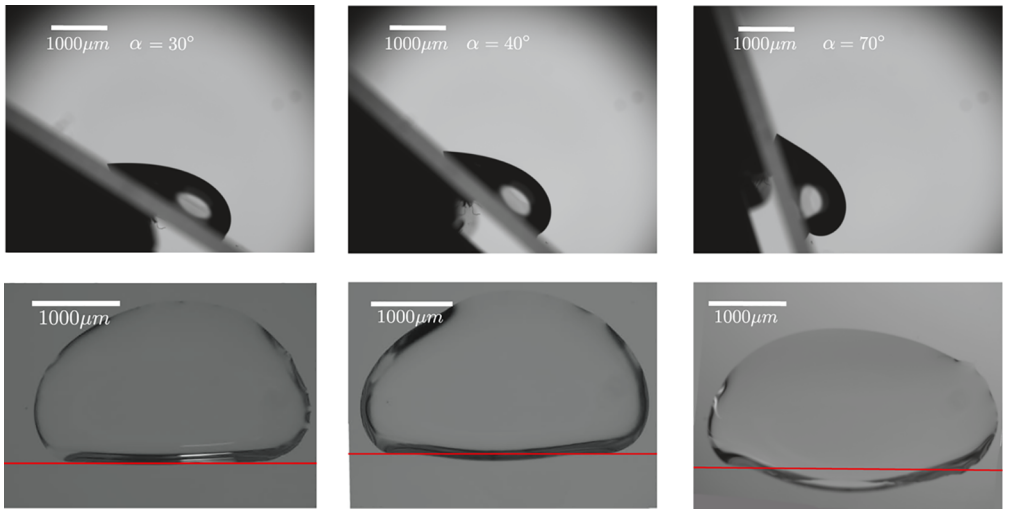

Figure 1. Corresponding experimental side (top) and bottom (bottom) views of a 60 μL water droplet (corresponding to a Bond number of Bo = 2.06) on a "chemical step": the substrate inclination with respect to the horizontal plane for each pair of images is $\alpha = 30°$ (left), 40° (middle), and 70° (right). Note that the very same drop is seen in the images; it is only the tilting which changes. The hydrophilic part of the substrate glass was coated with 3-aminopropyltriethoxysilane (θ_u = 44 ± 2°), while the part below the chemical step was coated with hydrophobised silica nanoparticles (30 nm) in isopropanol solution (θ_d = 155 ± 3°). Note that because of irregular pinning effects, the bottom view is not symmetric, in contrast to what the theoretical treatment of the ideal case will give.

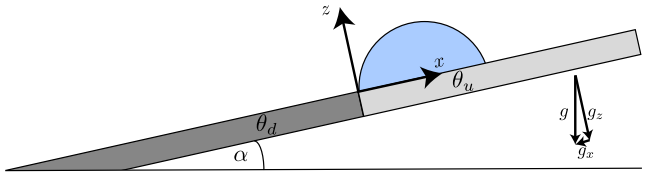

Figure 2. Properties of the system in which we are searching for stable shapes. The tilted substrate consists of two parts, in which Young's angles are θ_d and θ_u, respectively.

surface in the gravitational field. The substrate slope α denotes both the angle which the tilted substrate makes with the horizontal plane and the connection between the gravity force and its components in the x−z coordinate system. The tilted substrate consists of two parts, where the part below and above the chemical step respectively have the lyophobic Young's angle θ_d and the lyophilic Young's angle θ_u. Here, the indices d and u stand for down and up, respectively. In the case of $\theta_d < \theta_u$, the droplet would prefer to travel down the chemical step even without the gravity, so we will explore the phase space where $\theta_d > \theta_u$. Note that in our approach, we totally neglect contact angle hysteresis, as we ascribe only one contact angle to each side of the substrate, that is, advancing and receding contact angle are assumed to be identical, namely, they both have the value of the Young angle.

The aim of this paper is to clarify under what conditions a stable equilibrium shape exists for a sessile droplet at a chemical step experiencing a body force acting. The dynamics of this system has recently been explored by various other authors;[23−28] however, it was done by using the local contact line hysteresis laws. The common name for such dynamical models is "contact line friction methods" (CLFM).[25,29] The method can produce stable drop shapes which were experimentally confirmed by Semprebon et al.[26] In the present work, the hysteresis effect is replaced with the droplet contact energy contribution to the droplet interfacial energy because we assume that the droplet interface is locally in mechanical equilibrium (i.e., the advancing and the receding contact angle equal each other and take the value of Young's angle).

The paper is organized as follows: we will first explain the theoretical framework for the case for which only the tangential body force component plays a role. Then, we will extend this framework to also include the normal force component. After explaining the numerical details, we will present the results for the equilibrium droplet shape and culminating in threshold values for the force beyond which the droplet will start to move. The paper ends with conclusions and an outlook.

■ ENERGY FUNCTIONALS

Omission of the Normal Gravity Component. In this section, we assume that only the tangential force component plays a role, which for comparison with the more general case, we already call $g_x = g \sin \alpha$. To write down the total droplet energy, we must combine both interfacial and gravitational contributions, which results in

$$E = \gamma_{vl}A_{vl} + (\gamma_{sl}(x) - \gamma_{sv}(x))A_{sl} + \rho g_x \int_V x \, dV \tag{1}$$

where γ and A respectively denote surface tension and interfacial area, while their indices indicate between which two phases the surface tension and the interfacial area are defined, where s stands for solid (substrate), l for the liquid of the droplet, and v is used for the outer (e.g., vapor) phase. The last term on the right side of the equation is the potential energy of the droplet under the influence of the body force, where ρ is the droplet density and V the droplet volume. To nondimensionalize eq 1, we divide the whole equation by the surface tension γ_{vl} and the square value of volume length scale $l_V \equiv V^{1/3}$ and obtain

$$\tilde{E} \equiv \frac{E}{\gamma_{vl} l_V^2} = \tilde{A}_{vl} - \cos\ \theta_Y(\tilde{x})\tilde{A}_{sl} + Bo_x \int_{\tilde{V}} \tilde{x} \, d\tilde{V} \tag{2}$$

where we have used Young's law for the equilibrium contact angle

DOI: 10.1021/acs.langmuir.8b03557
Langmuir 2019, 35, 3880−3886

$$\cos\ \theta_Y(\tilde{x}) = \frac{\gamma_{sv}(\tilde{x}) - \gamma_{sl}(\tilde{x})}{\gamma_{vl}} = \begin{cases} \theta_d, & \text{if } \tilde{x} \le 0 \\ \theta_u, & \text{if } \tilde{x} > 0 \end{cases} \quad (3)$$

and we have introduced the Bond number $Bo_x = \rho g_x {l_V}^2/\gamma_{vl}$, where index x indicates that it is defined with the respect to the tangential body force acceleration. It simply represents the tangential body force. Dimensionless quantities are labeled by tildes. By choosing the volume length scale as a characteristic length scale, we perform the minimization of the eq 2 on the unit volume. Because of this, instead of looking at the Bond number as the ratio between capillary and gravitational forces, it is more convenient to think of the Bond number as a squared ratio between the capillary and the volume length scale because it can be expressed as $Bo_x = {l_V}^2/{l_{cx}}^2$, where l_{cx} is the capillary length scale $l_{cx} = \sqrt{\gamma_{vl}/\rho g_x}$ determined by the influence of the tangential gravity component g_x. The second term in the dimensionless energy, the contact energy term, is qualitatively different from what occurs in the CLFM because this term is used instead of the local contact angle hysteresis laws. In the CLFM method, minimization of the dimensionless energy without the contact energy term is performed, while the contact line is fixed and afterward one would fix the interface position and update the contact line position by the hysteresis law. This process is repeated until the stable shape is obtained. In our calculation, we minimize the dimensionless energy in a single step. The local contact angle in the CLFM method has an allowed range between the receding and the advancing contact angle and there is a hysteresis force locally acting on the contact line. When the droplet reaches the stable state, the net local hysteresis force along the contact line is a force with the opposite direction and the same value as the body force applied to the droplet.[25] Locally, the contact angle in our calculation is in a mechanical equilibrium, which implies that the local contact angle always equals $\theta_Y(\tilde{x})$. Note that this also holds at the chemical step, where the contact angle is in mechanical equilibrium for any value of the contact angle between θ_u and θ_d. The mechanical equilibrium of the outer interface is the same in both the CLFM and in our calculation because the curvature has to satisfy the Young−Laplace equation, which reads

$$2\gamma\kappa = \Delta p - \rho x g_x \quad (4)$$

where Δp is the pressure jump across the interface at $x = 0$ and κ is the mean interface curvature. In a nondimensional form, eq 4 reads

$$2\tilde{\kappa} = \Delta\tilde{p} - Bo_x\tilde{x} \quad (5)$$

where $\Delta\tilde{p} = l_V\Delta p/\gamma_{vl}$ denotes the dimensionless pressure jump at $\tilde{x} = 0$. Although in eq 5 we are expressing the mechanical equilibrium, the important geometrical result is that $\partial\tilde{\kappa}/\partial\tilde{x} = -Bo_x/2$, which will have a dominant effect in the cases of small values of θ_u because the droplet will try to spread itself on the substrate, increasing the range of values of $\tilde{x}$ for the contact line. In general, the value of $\Delta\tilde{p}$ cannot be obtained analytically.

Inclusion of the Normal Gravity Component. We now include the normal force to the problem, expressed as normal gravity component $g_z = g\cos\alpha$. To include this interaction in the energy functional, we must add one term to the right hand side of eq 1, which results in

$$E = \gamma_{vl}A_{vl} + (\gamma_{sl}(x) - \gamma_{sv}(x))A_{sl} + \rho g_x\int_V x\ dV + \rho g_z\int_V z\ dV \quad (6)$$

Equation 6 is nondimensionalized with the volume length scale l_V as the characteristic length scale and outer surface tension γ_{vl} as the characteristic surface tension. The resulting dimensionless equation is

$$\tilde{E} \equiv \frac{E}{\gamma_{vl}{l_V}^2} = \tilde{A}_{vl} - \cos\theta_Y(\tilde{x})\tilde{A}_{sl} + Bo_x\int_{\tilde{V}}\tilde{x}\ d\tilde{V} + Bo_z\int_{\tilde{V}}\tilde{z}\ d\tilde{V} \quad (7)$$

Similar to the Young−Laplace equation (eq 4), the curvature κ has to follow

$$2\gamma\kappa = \Delta p - \rho x g_x - \rho z g_z \quad (8)$$

which in the dimensionless form becomes

$$2\gamma\kappa = \Delta p - \rho x g_x - \rho z g_z \quad (9)$$

where $\Delta p\tilde{x}$ is now the pressure at $x = z = 0$. In this case, the curvature has to satisfy two geometrical relations, namely, $\partial\tilde{\kappa}/\partial\tilde{x} = -Bo_x/2$ and $\partial\kappa/\partial\tilde{z} = -Bo_z/2$. We can express the total Bond number Bo as

$$Bo = \frac{\rho g {l_V}^2}{\gamma_{vl}} = \sqrt{{Bo_x}^2 + {Bo_z}^2} \quad (10)$$

We can thus express the parameter space either via (Bo_x,Bo_z) or via (Bo,α).

Numerical Details. To minimize eqs 2 and 7 under the unit volume constraint, we have used Surface Evolver,[21,22] which is a free energy minimization software, which represents interfaces through a triangular mesh and locally moves triangle vortices in the energy descent direction. We initialize the cube with the unit volume and position it such that the one side of the cube lies in the plane $\tilde{x} = 0$, while the rest of the cube is above the lyophilic part $\tilde{x} > 0$. Initially, we let Surface Evolver minimize the energy functional without gravity terms for a few times to relax the initial shape, which leads to a spherical caplike shape where the contact line is positioned partially on the lyophilic part of the substrate $\tilde{x} > 0$ and partially on the chemical step. Afterwards, we include the body force to the droplet and let the system equilibrate. To detect stable shapes, we repeat series of energy minimizations, followed up with refinement of the mesh, until the difference in energy between two cycles becomes less than 0.005%. When the convergence reaches the target value, we check the stability of the solution by introducing a stochastic noise along the interface and let the process repeat itself. Using the above described algorithm, we have determined threshold values of the Bond number Bo_t for which stable solutions are still obtainable with the bisection method. Throughout the calculation, refinement of the triangular mesh is done in the way that we introduce the dimensionless length scale l_{mesh} and split edges whose length is longer than l_{mesh}, while we delete all the edges smaller than $0.4l_{mesh}$. In all calculations, we keep the value of l_{mesh} set to 0.1.

RESULTS

Omission of the Normal Gravity Component. We will firstly explore properties of stable droplet shapes when the

DOI: 10.1021/acs.langmuir.8b03557
Langmuir 2019, 35, 3880−3886

normal gravity component g_z is neglected. In Figure 3, we show examples of such shapes for the respective values of Young'

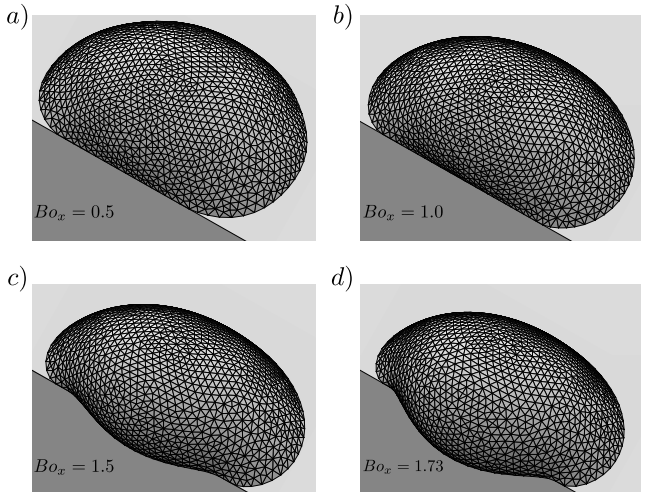

Figure 3. Series of shapes for Young's angles values of $\theta_d = 120°$ (darker part of the substrate) and $\theta_u = 60°$, for different values of Bond numbers. The threshold Bond number is $Bo_t = 1.735$ for given values of Young's angles. The camera position is the same in every image, but as visible droplets can migrate a little in the direction perpendicular along the chemical step which separates lyophobic and lyophilic parts of the substrate (denoted with same colors as in Figure 2.) because this does not change the value of the total energy. Note that for better visualization, the angle of view employed here is not the rectangular top view as in the experiments (Figure 1, 2nd row), but slightly tilted.

angle set to $\theta_u = 60°$ and $\theta_d = 120°$ because we can describe what is qualitatively happening with the droplet shape once we start increasing Bo_x. For $Bo_x = 0$, the droplet will form a spherical cap in the region $\tilde{x} > 0$ with the contact angle θ_u. Once we introduce the tangential body force to the system, a part of the contact line moves to the chemical step and the local contact angle on the chemical step ranges from θ_u to θ_d. As visible in Figure 3a,b, for small Bond numbers, the front part of the contact line is positioned on the chemical step and as we increase the Bond number, the droplet is pushed toward the lyophobic side. Eventually, a part of the contact line will leave the chemical step and start to spread on the lyophobic area with the constant contact angle θ_d, while the remaining part of the contact line still remains on the chemical step, as visible in Figure 3c. This behavior of the contact line and the contact angle is completely analogous to the droplet wetting of a single chemical pattern, without the body force applied to the droplet.[10−14] This behavior is very different from the CLFM method because the contact line will not cancel out the body force applied to the droplet itself,[25] but rather the stable shapes are realized via a self-deformation where the mechanical equilibria of the contact line and the interface are satisfied.

In Figure 3d, we show the stable morphology close to the threshold Bond number Bo_t, which is the largest Bond number for which the equilibrium shape is observed. For the given value of Young's angles ($\theta_u = 60°$ and $\theta_d = 120°$), the threshold Bond number is $Bo_t = 1.735$. A numerical problem which arises around the threshold Bond number is that the part of the contact line which is positioned on the chemical step becomes so small that the droplet morphology cannot realize the transition from the value of the local contact angle θ_u to θ_d along that part of the contact line. The stable smooth morphology, which satisfies the mechanical equilibria expressed via Young's angle (eq 3) and the Young−Laplace equation (eq 5), cannot be obtained. For the values close to the threshold Bond number Bo_t, Surface Evolver cannot resolve the smooth transition of the contact angle along the chemical step, but if we apply a small transitional shift to the droplet morphology toward the negative x-direction, the whole morphology can retreat back to its original shape, indicating that the local energy minimum is present, but the transition is below the length scale of our mesh.

The above described contact line behavior toward the threshold equilibrium shape is not the same once the value of θ_u becomes relatively small compared to the value of θ_d. In Figure 4, we show the threshold shape for a system of values θ_d

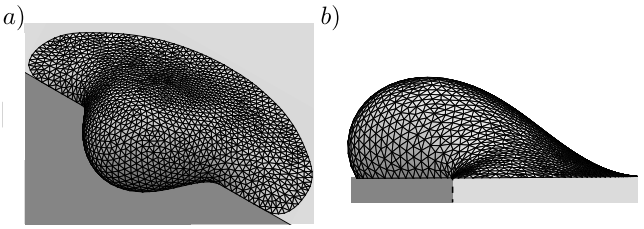

Figure 4. Threshold shape for Young's angles values of $\theta_d = 120°$ and $\theta_u = 10°$ for a value of the threshold Bond number $Bo_t = 3.232$ from a tilted view (a, same perspective as the previous figure) and $x-z$ cross-sectional (side) view of the droplet in which the striped line represents $x = 0$ plane (b).

= 120° and $\theta_u = 10°$. We see that the contact line length on the chemical step is still substantial. However, once we observe the droplet shape from a side view, we see that the droplet cross section has an inflection point and that the value of the curvature on the back end of the droplet is negative. If we increased the Bond number, a part of the triangulation mesh would sink below the substrate ($z < 0$) because of the increased curvature gradient along the x-axis, which is unphysical. Mathematically, it indicates that there may be geometrical shapes which solve the Young−Laplace equation, but obviously these shapes are not physical as the substrate is impermeable. When we forced the mesh to stay above the substrate, the droplet shape would diverge. In Figure 5a, we show values of the threshold Bond number Bo_t (beyond which stable equilibria are no longer possible) as a function of the equilibrium contact angles θ_u and θ_d. The general rule for the threshold Bond number Bo_t is that it increases with increasing difference in the wettability, but the threshold Bond number is not only a function of $\theta_d - \theta_u$ because as we show on the threshold equilibrium shape in Figure 4, the droplet interface curvature also plays a role. For the case of $\theta_d = \theta_u$, there is no stable equilibrium shape, as this corresponds to the homogeneous case.

In the case of this subsection, when still neglecting the normal gravity component in the energy functional, we can even analytically calculate the relation between the size of the droplet and the maximum slope of the substrate α_{max} for which the droplet can form the equilibrium shape: from the requirement that $Bo_x \leq Bo_t$, we readily obtain

$$\sin \alpha < \frac{Bo_t l_c^2}{l_V^2} \tag{11}$$

DOI: 10.1021/acs.langmuir.8b03557
Langmuir 2019, 35, 3880−3886

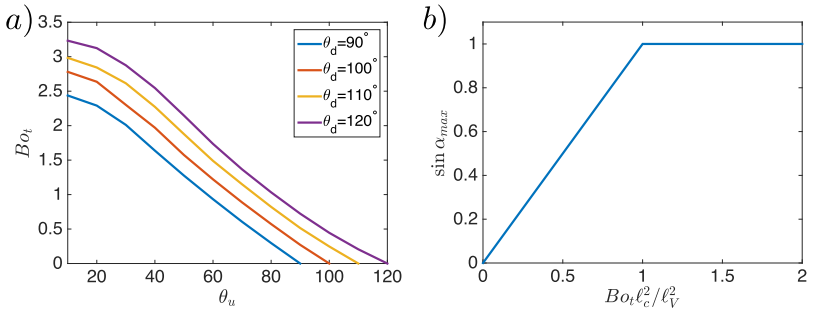

Figure 5. a) Threshold values Bo_t as a function of both Young's angles θ_u and θ_d. Once we obtain those values, we completely describe the range of the substrate slope α as a function of the size of the droplet in (b), where l_V denotes the volume length scale.

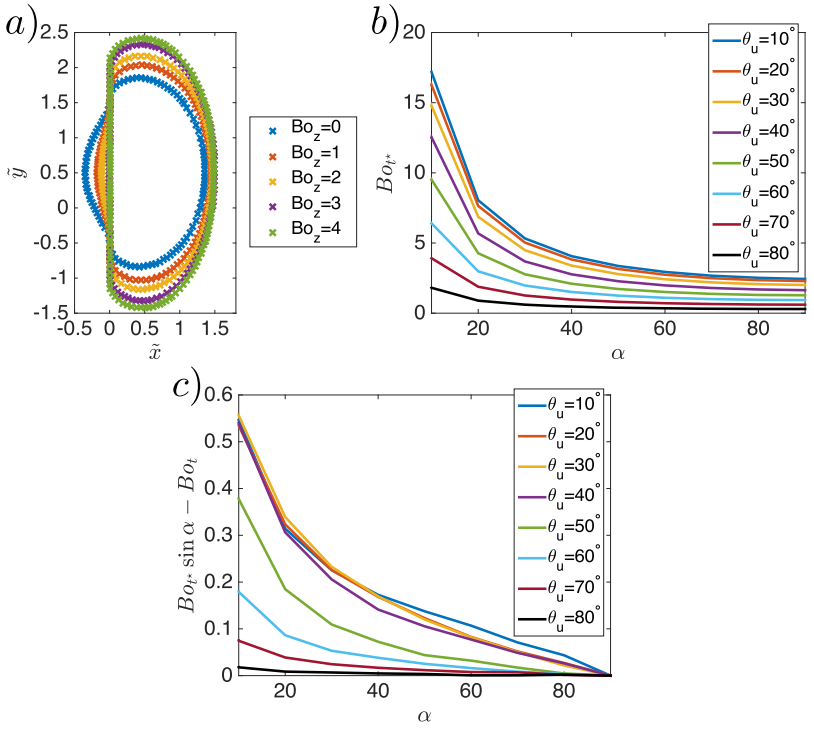

Figure 6. (a) Contact line position of stable droplet shapes for a fixed value of Bo_x and for the increasing Bo_z. $\tilde{y}$ denotes the spatial coordinate along the chemical step, but the energy functionals expressed in eqs 2 and 7 do not depend on it. (b) Threshold values Bo_t^* of the total Bond number Bo for which the droplet can still obtain an equilibrium shape. (c) Difference between the tangential gravity component Bo_t^* sin α and the threshold Bond number Bo_t (Figure 5a) for the case without the normal force component.

where $l_c \equiv \sqrt{\gamma_{vl}/\rho g}$ is the capillary length determined by the total value of the gravity acceleration g. For the case when $l_V < \sqrt{Bo_t}\,l_c$, the droplet has a stable shape for any given substrate slope α, but in the case of $l_V > \sqrt{Bo_t}\,l_c$, the fraction on the right hand side of the eq 11 has a value smaller than one. eq 11 implies a maximum substrate slope α_{max} with

$$\sin\alpha_{max} = \begin{cases} 1, & \text{if } l_V < \sqrt{Bo_t}\,l_c \\ \dfrac{Bo_t l_c^{\,2}}{l_V^{\,2}}, & \text{if } l_V > \sqrt{Bo_t}\,l_c \end{cases} \qquad (12)$$

$\sin\alpha_{max}$ is shown in Figure 5b.

With the result shown in Figure 5, we have completely solved the problem of threshold values for the case of the energy functional expressed in eq 2, for both the droplet size and the substrate slope.

Inclusion of the Normal Gravity Component. From now on, we are going to include the effect of the normal gravity component g_z. Because we are now introducing one more parameter (either Bo_z or α) to our analysis, we will limit our attention to cases with the fixed value of the lyophobic Young's angle $\theta_d = 90°$, while we will still change the value of the lyophilic Young's angle $10° \le \theta_u \le 90°$, where the case of $\alpha = 90°$ was already previously calculated and summarized in Figure 5a. In Figure 6a, we show what happens with the contact line for the unit volume droplet, once we fix the value of $Bo_x = 1.5$ and change the value of Bo_z, for the lyophilic Young's angle $\theta_u = 40°$. Intuitively, one would expect for the increasing value of Bo_z that the droplet shape is going to be more spread and flat, but what we observe is that in this given system, the droplet contact line is retreating from the lyophobic part to the chemical step and the contact area with the lyophilic part increases. To observe threshold equilibrium shapes, once the full gravity effect is included, we define Bo_t^* as a threshold value of the total Bond number

DOI: 10.1021/acs.langmuir.8b03557
Langmuir 2019, 35, 3880−3886

Bo and in the Figure 6b, we show the value of Bo_t^* as a function of the substrate slope α and the lyophilic Young's angle θ_u. For the substrate slope value of $\alpha = 90°$, we just use the previously calculated threshold values of Bo_t. Once the difference between the Young angles becomes substantial, we observe that values of Bo_t^* go above 10. For the case of $\alpha = 0°$, the value of the threshold total Bond number Bo_t^* diverges because the equilibrium shape is a pancake-like morphology on the lyophilic part of the substrate. For almost perfectly wettable substrates and small substrate slopes, the droplets have equilibrium wetting shapes even with the volume length scale much larger than the capillary length scale. In Figure 6c, we show the difference between the tangential component of the threshold total Bond number Bo_t^* and the threshold Bond number Bo_t, which was calculated for the case of omission of the normal gravity component (Figure 5a). It is immediately clear that with the inclusion of the normal gravity component, the threshold tangential gravity component becomes larger because of the contact line effect explained in Figure 6a.

Larger droplets can also deform to the mechanical equilibrium because the droplet tends to retreat to the lyophilic part of the substrate with the increasing normal gravity component. The mechanism for the existence of the threshold volume is still the same as in the case of neglecting the normal gravity component (see previous subsection), but in this more general case, we could not achieve an analytical expression for the threshold.

CONCLUSIONS AND OUTLOOK

Equilibrium shapes of a droplet on the tilted substrate patterned with a chemical step are obtained using Surface Evolver. When disregarding normal forces (e.g., for droplets smaller than the capillary length), we could calculate the threshold volume for which the droplet will not be able to be at the chemical step, and we analytically connect this result to the maximum substrate slope for which the stable shapes can still be observed. Once we include normal forces, we observe that for the same value of the tangential component, the normal component helps the droplet to retreat to the lyophilic part of the substrate. Qualitatively, we show that in the case of a large difference between the two Young angles, it is the Young–Laplace equation which causes the existence of the threshold droplet volume for which the stable shapes can be observed, while in the case of a small difference in wettability, we identify that the mechanical equilibrium of the contact line cannot be satisfied without singularities present at the contact line.

Obviously, a direct and quantitative one-to-one comparison of our theoretical results with experiments would be desirable. However, given the practical difficulties in producing substrates without any contact line hysteresis and without any heterogeneities, this is presently extremely difficult.

Finally, we stress again that, while we explain our results on the example of the gravity interaction with the droplet, our work can also be interpreted for many other situations in which one has a body force acting on a droplet, including exclusively wall-parallel body forces.

AUTHOR INFORMATION

Corresponding Author

*E-mail: d.lohse@utwente.nl.

ORCID

Ivan Dević: 0000-0003-0977-9973

Detlef Lohse: 0000-0003-4138-2255

Notes

The authors declare no competing financial interest.

ACKNOWLEDGMENTS

This work was supported by the Netherlands Center for Multiscale Catalytic Energy Conversion (MCEC), an NWO Gravitation programme funded by the Ministry of Education, Culture and Science of the government of the Netherlands.

REFERENCES

(1) Good, R. J. Contact angle, wetting and adhesion: a critical review. *J. Adhes. Sci. Technol.* **1992**, *6*, 1269–1302.

(2) de Gennes, P. G.; Brochard-Wyart, F.; Quere, D. *Capillarity and Wetting Phenomena: Drops And Bubbles And Pearls And Waves*; Springer: New York, 2004.

(3) de Gennes, P. G. Wetting: statics and dynamics. *Rev. Mod. Phys.* **1985**, *57*, 827.

(4) Herminghaus, S.; Brinkmann, M.; Seemann, R. Wetting and Dewetting of Complex Surface Geometries. *Annu. Rev. Mater. Res.* **2008**, *38*, 101–121.

(5) Soltman, D.; Smith, B.; Kang, H.; Morris, S. J. S.; Subramanian, V. Methodology for Inkjet Printing of Partially Wetting Films. *Langmuir* **2010**, *26*, 15686–15693.

(6) Lee, T.; Charrault, E.; Neto, C. Interfacial slip on rough, patterned and soft surfaces: A review of experiments and simulations. *Adv. Colloid Interface Sci.* **2014**, *210*, 21–38.

(7) Clausen, B. S.; Schiøtz, J.; Gråbæk, L.; Ovesen, C. V.; Jacobsen, K. W.; Nørskov, J. K.; Topsøe, H. Wetting/ non-wetting phenomena during catalysis: Evidence from in situ on-line EXAFS studies of Cu-based catalysts. *Top. Catal.* **1994**, *1*, 367–376.

(8) Hu, H.; Wen, J.; Bao, L.; Jia, L.; Song, D.; Song, B.; Pan, G.; Scaraggi, M.; Dini, D.; Xue, Q.; Zhou, F. Significant and stable drag reduction with air rings confined by alternated superhydrophobic and hydrophilic strips. *Sci. Adv.* **2017**, *3*, No. e1603288.

(9) Marmur, A. Contact Angle Hysteresis on Heterogeneous Smooth Surfaces. *J. Colloid Interface Sci.* **1994**, *168*, 40–46.

(10) Dević, I.; Soligno, G.; Dijkstra, M.; van Roij, R.; Zhang, X.; Lohse, D. Sessile nanodroplet on elliptical patches of enhanced lyophilicity. *Langmuir* **2017**, *33*, 2744–2749.

(11) Brinkmann, M.; Lipowsky, R. Wetting morphologies on substrates with striped surface domains. *J. Appl. Phys.* **2002**, *92*, 4296–4306.

(12) Darhuber, A. A.; Troian, S. M.; Miller, S. M.; Wagner, S. Morphology of liquid microstructures on chemically patterned surfaces. *J. Appl. Phys.* **2000**, *87*, 7768–7775.

(13) Extrand, C. W. Contact Angles and Hysteresis on Surfaces with Chemically Heterogeneous Islands. *Langmuir* **2003**, *19*, 3793–3796.

(14) Lenz, P.; Lipowsky, R. Morphological Transitions of Wetting Layers on Structured Surfaces. *Phys. Rev. Lett.* **1998**, *80*, 1920–1923.

(15) Brandon, S.; Haimovich, N.; Yeger, E.; Marmur, A. Partial wetting of chemically patterned surfaces: The effect of drop size. *J. Colloid Interface Sci.* **2003**, *263*, 237–243.

(16) Gao, L.; McCarthy, T. J. How Wenzel and Cassie Were Wrong. *Langmuir* **2007**, *23*, 3762–3765.

(17) McHale, G. Cassie and Wenzel: Were They Really So Wrong? *Langmuir* **2007**, *23*, 8200–8205.

(18) Matsui, H.; Noda, Y.; Hasegawa, T. Hybrid Energy-Minimization Simulation of Equilibrium Droplet Shapes on Hydrophilic/Hydrophobic Patterned Surfaces. *Langmuir* **2012**, *28*, 15450–15453.

(19) Soligno, G.; Dijkstra, M.; van Roij, R. The equilibrium shape of fluid-fluid interfaces: Derivation and a new numerical method for Young?s and Young–Laplace equations. *J. Chem. Phys.* **2014**, *141*, 244702.

DOI: 10.1021/acs.langmuir.8b03557
Langmuir 2019, 35, 3880–3886

(20) Nguyen, C. T.; Barisik, M.; Kim, B. Wetting of chemically heterogeneous striped surfaces: Molecular dynamics simulations. *AIP Adv.* **2018**, *8*, 065003.
(21) Brakke, K. A. The Surface Evolver. *Exp. Math.* **1992**, *1*, 141−165.
(22) Surface Evolver Manual, version 2.70, 2013; http://facstaff.susqu.edu/brakke/evolver/downloads/manual270.pdf.
(23) Varagnolo, S.; Schiocchet, V.; Ferraro, D.; Pierno, M.; Mistura, G.; Sbragaglia, M.; Gupta, A.; Amati, G. Tuning Drop Motion by Chemical Patterning of Surfaces. *Langmuir* **2014**, *30*, 2401−2409.
(24) Varagnolo, S.; Ferraro, D.; Fantinel, P.; Pierno, M.; Mistura, G.; Amati, G.; Biferale, L.; Sbragaglia, M. Stick-Slip Sliding of Water Drops on Chemically Heterogeneous Surfaces. *Phys. Rev. Lett.* **2013**, *111*, 066101.
(25) Semprebon, C.; Brinkmann, M. On the onset of motion of sliding drops. *Soft Matter* **2014**, *10*, 3325−3334.
(26) Semprebon, C.; Varagnolo, S.; Filippi, D.; Perlini, L.; Pierno, M.; Brinkmann, M.; Mistura, G. Deviation of sliding drops at a chemical step. *Soft Matter* **2016**, *12*, 8268−8273.
(27) Sbragaglia, M.; Biferale, L.; Amati, G.; Varagnolo, S.; Ferraro, D.; Mistura, G.; Pierno, M. Sliding drops across alternating hydrophobic and hydrophilic stripes. *Physical Review E: Statistical, Nonlinear, and Soft Matter Physics* **2014**, *89*, 012406.
(28) Lv, C.; Shi, S. Wetting states of two-dimensional drops under gravity. *Phys. Rev. E* **2018**, *98*, 042802.
(29) Santos, M. J.; Velasco, S.; White, J. A. Simulation Analysis of Contact Angles and Retention Forces of Liquid Drops on Inclined Surfaces. *Langmuir* **2012**, *28*, 11819−11826.

DOI: 10.1021/acs.langmuir.8b03557
Langmuir 2019, 35, 3880−3886